BMC Pulmonary Medicine

RESEARCH

Open Access

A novel pulmonary fibrosis NOD/SCID murine model with natural aging

Zhaoxia Ma[1†], Lihua Qiu[1†], Jianxiu Sun[2], Zhen Wu[3], Shu Liang[1], Yunhui Zhao[2], Jinmei Yang[2], Shijun Yue[1], Min Hu[1*] and Yanjiao Li[1*]

Abstract

Background Idiopathic pulmonary fibrosis (IPF) is an age-related disease severely affecting life quality with its prevalence rising as the population ages, yet there is still no effective treatment available. Cell therapy has emerged as a promising option for IPF, however, the absence of mature and stable animal models for IPF immunodeficiency hampers preclinical evaluations of human cell therapies, primarily due to rapid immune clearance of administered cells. This study aims to establish a reliable pulmonary fibrosis (PF) model in immunodeficient mice that supports autologous cell therapy and to investigate underlying mechanism.

Methods We utilized thirty 5-week-old male NOD/SCID mice, categorizing them into three age groups: 12weeks, 32 weeks and 43 weeks, with 6 mice euthanized randomly from each cohort for lung tissue analysis. We assessed fibrosis using HE staining, Masson's trichrome staining, α-SMA immunohistochemistry and hydroxyproline content measurement. Further, β-galactosidase staining and gene expression analysis of *MMP9*, *TGF-β1*, *TNF-α*, *IL-1β*, *IL-6*, *IL-8*, *SOD1*, *SOD2*, *NRF2*, *SIRT1*, and *SIRT3* were performed. ELISA was employed to quantify protein levels of TNF-α, TGF-β1, and IL-8.

Results When comparing lung tissues from 32-week-old and 43-week-old mice to those from 12-week-old mice, we noted a marked increase in inflammatory infiltration, fibrosis severity, and hydroxyproline content, alongside elevated expression levels of α-SMA and MMP9. Notably, the degree of fibrosis intensified with age. Additionally, β-galactosidase staining became more pronounced in older mice. Quantitative PCR analyses revealed age-related, increases in the expression of senescence markers (*GLB1*, *P16*, *P21*), and proinflammatory genes (*TGF-β1*, *TNF-α*, *IL-1β*, *IL-6*, *and IL-8*). Conversely, the expression of anti-oxidative stress-related genes (*SOD1*, *SOD2*, *NRF2*, *SIRT1*, and *SIRT3*) declined, showing statistically significant differences ($^{*}P < 0.05$, $^{**}P < 0.01$, $^{***}P < 0.001$). ELISA results corroborated these findings, indicating a progressive rise in the protein levels of TGF-β1, TNF-α, and IL-8 as the mice aged.

Conclusions The findings suggest that NOD/SCID mice aged 32 weeks and 43 weeks effectively model pulmonary fibrosis in an elderly context, with the disease pathogenesis likely driven by age-associated inflammation and oxidative stress.

†Zhaoxia Ma and Lihua Qiu contributed equally to this work.

*Correspondence:
Min Hu
huminynkm@163.com
Yanjiao Li
YanjiaoLi1688@126.com

Full list of author information is available at the end of the article

Keywords Natural aging, NOD/SCID mice, Pulmonary fibrosis model

Background

Idiopathic pulmonary fibrosis (IPF) is a chronic, progressive interstitial lung disease characterized by limited treatment options and a generally poor prognosis [1]. Animal models are indispensable for the study of human IPF. Commonly utilized species include mice, rats, rabbits, pigs, sheep, tree shrews, and non-human primates [2–7]. Large animals, such as pigs and monkeys, offer advantages due to their large body size and lung tissue, allowing for dynamic observed under non-invasive imaging techniques. However, the complexity and high costs associated with their use limit their widespread application [8, 9]. In contrast, mice are favored for PF studies due to their small size, light weight, and cost-effectiveness [10]. Aging is recognized as a primary pathogenic factor in IPF, significantly influencing its progression and prognosis [11]. Older animals typically demonstrate PF-related phenotypes more accurately than their younger counterparts, yet studies using naturally aging mice are scarce, primarily due to the high costs of long-term care [12]. Most research into PF mechanisms or pharmaceutical interventions employs young mice (aged 6–8 weeks), induced with agents like bleomycin, silica, radiation, or hypoxia to establish disease models. However, these models often fail to mimic the intricacies of human IPF and its association with aging. Recent years have seen a surge in preclinical exploring mesenchymal stem cells (MSCs) for IPF intervention, showcasing rapid advancements and promising clinical potential [13, 14]. MSCs are particularly noted for their immune-modulating and tissue remodeling capabilities [15]. Moreover, autologous stem cells, which are less likely to be eliminated by the immune system, have shown prolonged survival post-transplantation and greater efficacy in their secretory and cell differentiation functions [16], enhancing their clinical relevance. However, in preclinical studies investigating autologous stem cell intervention for IPF, mouse models with intact immune function can clear implanted human cells, thus hindering an accurate assessment of the intervention's effectiveness [17]. Immunodeficient animal models offer advantages in this context, althoug there are no existing reports of successful replicating the human IPF model in such animals. NOD/SCID mice, derived from a backcross between SCID mice and non-obese diabetic mice, exhibit low levels of natural killer (NK) cells and a deficiency in complement C5. These traits contribute to higher survival rates of human cells and grafts [18]. To date, NOD/SCID mice have been successfully used to model natural ovarian aging, patient-derived xenografts, leukemia, myeloma, retinoblastoma, and other human diseases [19–23]. In this study, 12-week-old NOD/SCID mice served as normal controls, while the feasibility of using naturally aging 32-week-old and 43-week-old NOD/SCID mice as models for human IPF was evaluated. This research aims to establish a suitable animal model for studying the efficacy of pharmaceutical agents designed to target IPF in humans.

Materials and methods

Experimental animals and experimental design

Thirty male NOD/SCID mice, aged 5 weeks were procured from GemPharmatech Co., Ltd. and were housed in a specific pathogen-free (SPF) facility. The environmental conditions were maintained at approximately 25 °C, with a relative humidity of 40–60%, and a 12-hour light-dark cycle. At 12, 32, and 43 weeks of age, we randomly euthanized six mice from each group using cervical dislocation after isoflurane (RWD, China) overdose. Specifically, Mice were placed in a clear plastic induction box, where 5% isoflurane gas mixed with O_2 was delivered at a flow rate of 1.0 L/min. The mice stayed in the induction box for approximately 3 to 4 min until they were euthanized. One mouse was placed in the induction box individually. All mice underwent cervical dislocation immediately after they were euthanized [24]. The left lung tissue was fixed in a 4% paraformaldehyde (PFA) solution for pathological examination, while the right lung tissue was snap-frozen in liquid nitrogen and stored at -80 °C for molecular analysis. All experimental protocols and procedures received approved from the Experimental Animal Welfare and Ethics Committee of Kunming University (approval number: 2021kmu011). Due to the risk of natural mortality among NOD/SCID mice during the experiment, any mice that died naturally were treated humanely. The remaining mice were euthanasia using isoflurane (RWD, China) overdose and cervical dislocation, ensuring they were treated with care throughout the process.

Paraffin sections of lung tissue

Following fixation in 4% PFA for a minimum of 24 h, the left lung tissue was subjected to a stepwise process using various concentrations of ethanol, followed by clarification in xylene. The cleared tissue was then immersed in paraffin wax at 60 °C twice, with each immersion lasting 90 min, to facilitate tissue embedding. Section 4 μm thickness were obtained using a paraffin microtome (Huahai, HHQ-3558).

HE staining and ashcroft scoring

The paraffin sections were dried overnight in an oven at 37 °C, dewaxed in xylene, and subsequently rehydrated

through a gradient of ethanol concentrations. Staining was performed according to the instructions provided by the HE staining kit (Solarbio, G1120) and the stained slides were scanned using a research-grade whole slide scanning system (Olympus, VS200). The results of the HE staining were evaluated using the Ashcroft scoring system [25]. For each group, six mice were selected, and three panoramic slides were chosen for each mouse. Scoring was conducted independently by two observers, and the average score for each mouse was calculated after summarizing the results.

Masson staining and positive area statistics

Collagen deposition in lung tissue sections was assessed using the Masson staining kit (Servicebio, GP1032) according to the manufacturer's instructions. Slide scanning was performed with the research-grade whole slide scanning system (Olympus, VS200), involving mice per group. For each mouse, five slides were selected, and each section was examined in 20 fields, avoiding areas with atmospheric tubes and large blood vessels. ImageJ software was utilized for statistical analysis of the blue-stained area, with the masson-stained positive area in lung tissue expressed as a percentage of the total lung area.

α-SMA immunohistochemistry

The paraffin sections were dewaxed using xylene and a gradient of ethanol. Antigen retrieval was performed by placing the sections in a citric acid antigen retrieval solution (pH 6.0) and subjecting them to microwave treatment at medium power for 8 min, followed by a pause for 8 min, and then heating at medium-low power for an additional 7 min. To block endogenous peroxidase activity, and the sections were incubated with hydrogen peroxide, followed by serum sealing. The sections were then incubated overnight at 4 °C with the primary antibody (Servicebio, GB111364, diluted in PBS at a ratio of α-SMA = 1:1000). Following this, the sections were incubated at room temperature for 50 min with the secondary antibody (HRP labeling Goat Anti-Rabbit IgG). Subsequent procedures included DAB color development, hematoxylin restaining of nuclei, dehydration, and clarification of the sections. Finally, the sections were mounted and scanned using a research-grade whole slide scanning system (Olympus, VS200). Each group included six mice, with three slides selected for each mouse. Image J software was utilized for statistical analysis of the α-SMA positive area, and the positive rate of α-SMA staining was expressed as the percentage of the positive area relative to the total lung area.

Hydroxyproline content detection

The hydroxyproline content in lung tissues from each group of animals was determined using a hydroxyproline assay kit (Nanjing Jiancheng, A030-2-1). Briefly, 30–50 mg of lung tissue was weighed and placed into a test tube, followed by the addition of 1 ml of alkali hydrolysate. The tissue was fully hydrolyzed in water at 95 °C. Samples were then processed according to the kit's instructions. The absorbance at 550 nm was measured using a Microplate System (TECAN, Infinite M200 pro), and the hydroxyproline content in each sample was calculated based on the formula provided in the kit.

Enzyme-linked immunosorbent assay

The protein expression levels of TGF-β1, TNF-α, and IL-8 in lung tissue were assessed using ELISA kits from EK-Bioscience, following the manufacturer's instructions. In brief, the lung tissues were weighed, and cold normal saline was added at a ratio of 1:250 (μg: ml) while kept on ice. After homogenizing the tissues, the mixture was centrifuged at 3000 rpm for 10 min, and the supernatant was collected according to the ELISA kit instructions for protein detection. Results were normalized to protein concentration using standards and controls included in the kit.

β-gal staining

After euthanasia, a portion of the left lung tissue was collected from the experimental mice. The tissue was fixed in 4% neutral formaldehyde solution for over 24 h, followed by dehydration using a gradient sucrose solution (15%, 20%, 30%). The tissue was then embedded in OCT and sliced into 10 μm sections using a frozen microtome (Thermo Fisher, HM525). Staining was performed according to the instructions provided in the β-gal staining kit (Beyotime, C0602), and the slides were scanned using a research-grade whole slide scanning system (Olympus, VS200). Six mice were selected for each group, with three slides chosen for each mouse. Image J software was utilized for statistical analysis of the positive area, and the positive rate of β-gal staining was expressed as the percentage of the positive area relative to the total lung area.

RNA extraction, reverse transcription and quantitative PCR

10–20 mg of right lung tissues were weighed, and RNA was extracted using the extraction method provided by Takara (9109). The RNA concentration was measured using an ultramicro nucleic acid protein analyzer (BioSpec-nano, Shimadzu, Japan). Subsequently, the RNA was reverse-transcribed into cDNA using a kit from Accurate Biology (AG11728), following the measured RNA concentration. Real-time fluorescence quantitative PCR was performed using SYBR qPCR SuperMix

Plus (Dib, QE006-02). The primers used for qPCR in this study are listed in Table 1, and the ΔΔCT analytical method was employed for comparative analysis.

Data statistics and analyes

The data from each experimental group were expressed as "mean ± standard deviation", and statistical analysis was conducted using SPSS 19.0 software. One-way ANOVA followed by Bonferroni's *post hoc* test was performed for comparisons among three groups. A *p*-value of less than 0.05 was considered to indicate a statistically significant difference.

Results

Changes in appearance and histology of lung tissue in experimental mice with increasing age

To assess whether the degree of pulmonary fibrosis in mice increases with age, we examined the appearance of lung tissue and performed HE and Masson staining on pathological sections from each group of mice. The results revealed distinct changes in lung tissue morphology associated with age. At 12 weeks, the lung tissue appeared smooth, moist, and exhibited a normal color (Fig. 1A). However, by 32 weeks, the lung tissue had turned black (Fig. 1B), and by 43 weeks, it became shriveled and smaller, with the entire lung tissue appearing black (Fig. 1C). HE staining of 12-week-old mice showed normal structure with no significant inflammation or fibrosis in the alveolar spaces or walls (Fig. 1D). In contrast, extensive structural changes were observed in the lungs of mice aged 32 and 43 weeks. Fibrosis was evident in both the alveolar walls and the alveolar spaces, displaying multifocal fibrosis. Additionally, compared to the 32-week-old mice, the 43-week-old mice exhibited a greater degree of fibrosis, increased infiltration of inflammatory cells in the lung tissue, rupture of the alveolar walls, and fusion of the alveolar cavities (Fig. 1E and F). The severity of lung fibrosis was assessed using the Ashcroft score. The scores for the 32-week-old and 43-week-old mice were significantly higher than those for the 12-week-old mice (**$P<0.01$) (Fig. 1J). Masson staining and the statistical analysis of positive area revealed that lung tissue from mice aged 32 and 43 weeks exhibited excessive deposition of collagen in the extracellular matrix (Fig. 1H and I). Compared to the 12-week-old group, the Masson staining positive area in both the 32-week-old and the 43-week-old groups increased significantly, with difference being statistically significant (*$P<0.05$, **$P<0.01$) (Fig. 1K).

Table 1 Primers used for qPCR in this study

Genes	Primers (5′-3′)
β-ACTIN	F: GTGACGTTGACATCCGTAAAGA
	R: GCCGGACTCATCGTACTCC
P16	F: CGCAGGTTCTTGGTCACTGT
	R: TGTTCACGAAAGCCAGAGCG
P21	F: ccttgtcgctgtcttgcactctg
	R: gctggtctgcctccgttttcg
GLB1	F: ACGCTGGACATCCTGGTGGAG
	R: CAGTTGGTGAGGACAGTGGAGTTG
IL-1β	F: tggcaactgttcctgaactcaactg
	R: tcatcttttggggtccgtcaacttc
IL-6	F: TAGTCCTTCCTACCCCAATTTCC
	R: TTGGTCCTTAGCCACTCCTTC
IL-8	F: acctgctctgtcaccgatgtctac
	R: caggcaaggtcagggcaaagaac
TNF-α	F: CAGGCGGTGCCTATGTCTC
	R: CGATCACCCCGAAGTTCAGTAG
TGF-β1	F: acaatggcggtgcggtcaag
	R: cagacttcatgcggcttctcacag
SOD1	F: agagcattccatcattggccgtac
	R: cgcaatcccaatcactccacagg
SOD2	F: caatctcaacgccaccgaggag
	R: agggctcaggtttgtccagaaaatg
SIRT1	F: actggagctggggtttctgtctc
	R: ggcttgagggtctgggaggtc
SIRT3	F: GGCTCTATACACAGAACATCGAC
	R: TAGCTGTTACAAAGGTCCCGT
NRF2	F: TCTTGGAGTAAGTCGAGAAGTGT
	R: GTTGAAACTGAGCGAAAAAGGC

Changes in α-SMA and Hydroxyproline content, and MMP9 gene expression in lung tissues of experimental mice with increasing age

Alpha-smooth muscle actin (α-SMA) serves as a marker for the transformation of fibroblasts into myofibroblasts. To further confirm that natural aging contributes to pulmonary fibrosis, we conducted an α-SMA immunohistochemical assay on lung tissues. The results indicated that, compared to the 12-week-old group, the expression of α-SMA in the damaged regions of the interstitial and alveolar spaces of the lung tissues in the 32-week-old and 43-week-old groups was elevated (Fig. 2A, B and C, arrowheads). The increase in α-SMA expression in the lung tissues of the 43-week-old group was statistically significant (**$P<0.01$) (Fig. 2D). Studies have indicated that abnormal lung remodeling in pulmonary fibrosis is characterized by increased expression of matrix metalloproteinase 9 (*MMP9*) [26]. In this study, we examined the changes in *MMP9* gene expression in lung tissues of mice from different age groups. The quantitative PCR results demonstrated that, compared to the 12-week-old group, the expression level of *MMP9* in the lung tissues of mice aged 32 and 43 weeks was elevated. Notably, the increase in *MMP9* gene expression in the 43-week-old was statistically significant (***$P<0.001$) (Fig. 2E). Additionally, hydroxyproline levels were higher in the 32-week-old and 43-week-old groups compared to the 12-week-old group

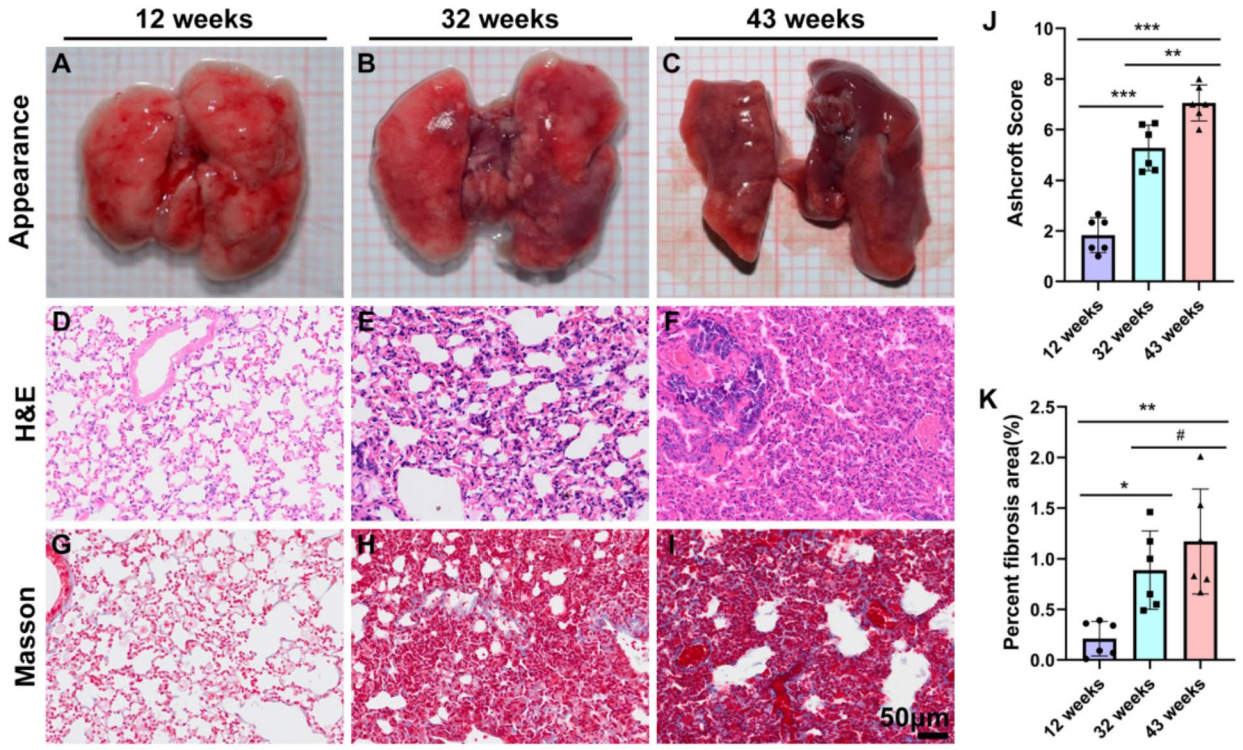

Fig. 1 illustrates the gradual increase in the degree of pulmonary fibrosis in experimental mice with advancing age. **A-C**: gross appearance of lung tissue; **D-F**: HE staining of lung tissue; **G-I**: Masson Trichrome staining of lung tissue; **J**: The severity of lung fibrosis was analyzed by Ashcroft score in the three groups; **K**: Masson's Trichrome positive areas of three groups were morphometrically quantified and represented as the percentage of total lung areas. Scale = 50 μm. Data are presented as the mean ± SEM ($n = 6$). $^{\#}P > 0.05$, $^{*}P < 0.01$, $^{**}P < 0.01$, $^{***}P < 0.001$.

(Fig. 2F), indicating that collagen content in lung tissue increased with the age of the mice.

Changes in β-gal staining and the expression of age-related genes in lung tissue of experimental mice with increasing age

The results of β-gal staining in the lung tissues indicated that the number of cells stained blue by β-gal at 12 weeks of age was minimal (Fig. 3A, arrowheads). However, the number of blue-stained cells in the lung tissue of mice at 32 and 43 weeks of age gradually increased with age (Fig. 3B and C, arrowheads). Compared to mice aged 12 weeks, the β-gal stained area in mice aged 32 and 43 weeks increased significantly ($^{*}P<0.05$, $^{***}P<0.001$) (Fig. 3D). The quantitative PCR results indicated that, relative to the 12-week-old mice, the expression levels of the β-gal encoding gene *GLB1* and senescence-related genes *P16* and *P21* in lung tissues of 43-week-old mice were elevated, with statistically significant differences ($^{***}P<0.001$). Furthermore, when comparing the 43-week-old mice to the 32-week-old mice, the expression of aging genes in lung tissues also showed statistically significant differences ($^{***}P<0.001$) (Fig. 3E, F and G).

Changes in the expression of pro-inflammatory related genes and proteins in lung tissues of experimental mice with age

The expression of pro-inflammatory genes in the lung tissues of experimental mice varied with age. Previous studies have shown an increase in the expression of inflammation-related genes in bleomycin-induced pulmonary fibrosis models [27]. In our study, we employed quantitative PCR to assess the expression of transforming growth factor β1 (TGF-β1), tumor necrosis factor α (TNF-α), interleukin-1β (IL-1β), interleukin-6 (IL-6), and interleukin-8 (IL-8) genes in the lung tissues of mice at various ages. The quantitative PCR results revealed that, compared to the 12-week-old mice, the expression levels of *TGFβ1*, *TNF-α*, *IL-6*, *IL-1β*, and *IL-8* genes were significantly elevated in the lung tissues of 43-week-old mice ($^{*}P<0.05$, $^{**}P<0.01$, $^{***}P<0.001$) (Fig. 4 A-E). Additionally, the protein expression levels of IL-8, TNF-α and TGF-β1 in the lung tissues from different groups by ELISA. The expression of TNF-α, TGF-β1 and IL-8 proteins were higher in the 32-week-old and 43-week-old groups compared to the 12-week-old group, but the difference of TNF-α, TGF-β1 was no statistically significant ($^{\#}P>0.05$) (Fig. 4 F-H).

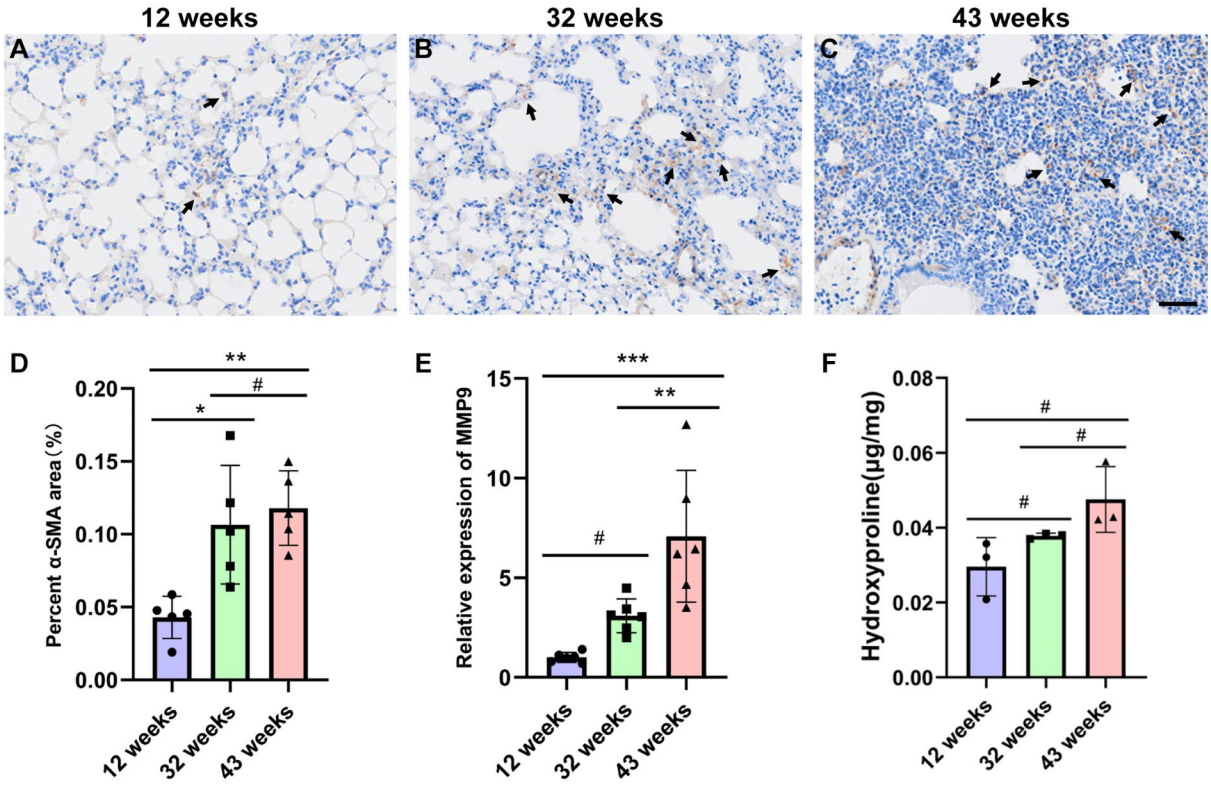

Fig. 2 illustrates the increased expression of α-SMA and *MMP9* genes in the lung tissue of experimental mice with advancing age. **A-C**: Representative images of α-SMA immunohistochemistry in lung tissue from mice aged 12 weeks (**A**), 32 weeks (**B**) and 43 weeks (**C**), with a scale bar of 50 μm and the arrows indicate positive areas; **D**: Immunohistochemical analysis of α-SMA in lung tissue; **E**: Quantitative PCR results for *MMP9* expression across the groups. Data are presented as the mean ± SEM ($n = 6$). $^{\#}P > 0.05$, $^{*}P < 0.05$, $^{**}P < 0.01$. **F**: Hydroxyproline content detection in each group. Data are presented as the mean ± SEM ($n = 3$). $^{\#}P > 0.05$.

The expression of anti-oxidative stress-related genes in lung tissues of experimental mice varied with age

Literature indicates that oxidative stress in lung tissue increases as mice age [28]. Oxidative stress, defined as the imbalance between reactive oxygen species (ROS) production and the antioxidant capacity of cells, is associated with fibrotic diseases, including pulmonary fibrosis [29]. The transcription factor NRF2 serves as the primary regulator of antioxidant genes in response to oxidative stress [30], while SOD1 and SOD2 are crucial antioxidant enzymes [31]. Additionally, SIRT1 and SIRT3 play protective roles against ROS [32]. In this study, we assessed the expression of antioxidative stress-related genes in lung tissues of NOD/SCID mice of varying ages. The quantitative PCR results demonstrated that, compared to the 12-week-old group, the expression levels of *SOD1*, *SOD2*, *NRF2*, *SIRT1*, and *SIRT3* genes in the lung tissues of the 32-week-old and 43-week-old groups were significantly decreased ($^{*}P < 0.05$, $^{***}P < 0.001$) (Fig. 5).

These results suggest that the antioxidant capacity of lung tissue decreases with the age of NOD/SCID mice.

Discussion

Idiopathic pulmonary fibrosis (IPF) is closely associated with aging, high morbidity rates, and poor prognosis. In recent years, significant progress has been made in understanding the mechanisms by which mesenchymal stem cells (MSCs) regulate immunity and tissue remodeling in animal models of pulmonary fibrosis [15]. Experimental studies have shown that MSCs can prevent and treat pulmonary fibrosis induced by bleomycin, silica, radiation, or hypoxia in animal models [33–36]. While these models are valuable for studying the development of pulmonary fibrosis, the pathogenesis of human IPF is highly complex. Consequently, these animal models cannot fully capture the natural progression of the disease in humans. Furthermore, animals with normal immune function can mount an immune response against implanted human cells, complicating the assessment of intervention efficacy. In this study, we utilized NOD/SCID mice of varying ages to simulate the lung tissue phenotypes associated with different stages of aging. This approach allowed us to assess the histological, pathological, and genomic changes associated with

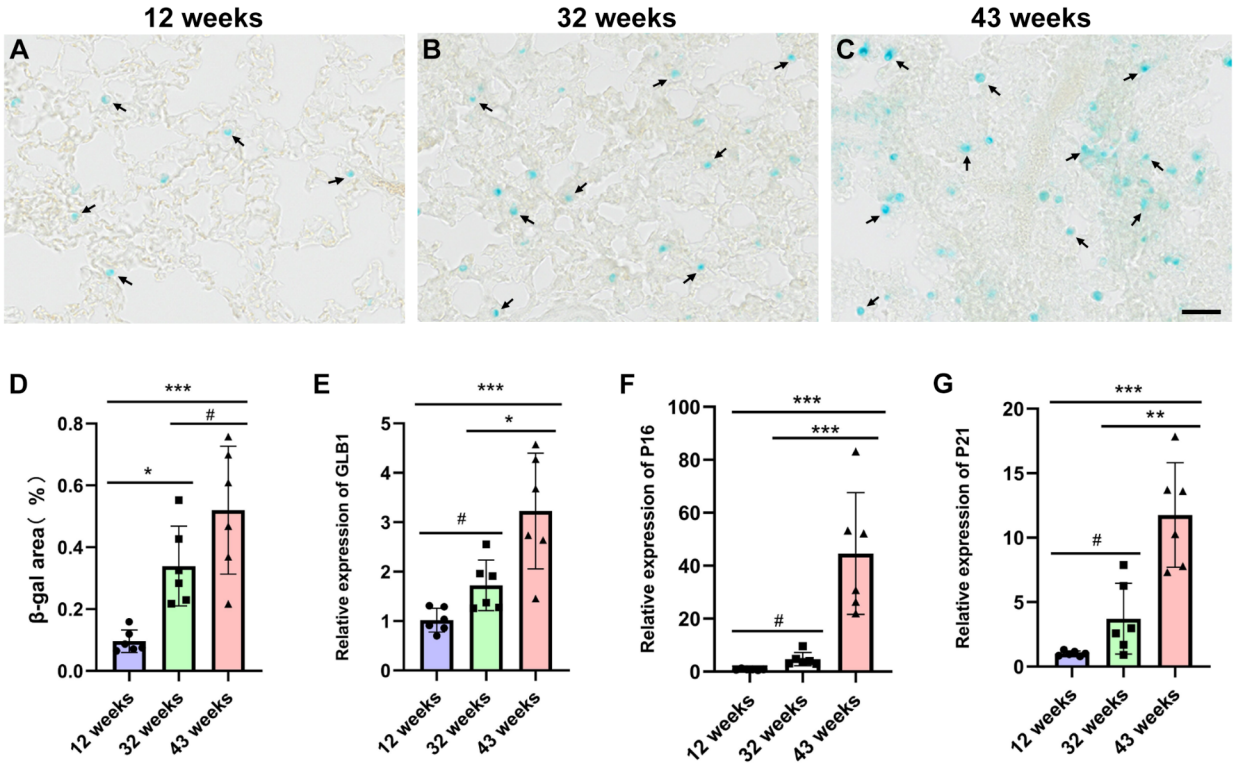

Fig. 3 illustrates that the degree of β-gal staining in the lung tissue of experimental mice intensified with increasing age, and the expression of age-related genes also increased correspondingly. **A-C**: Representative images of β-gal staining in lung tissue from mice aged 12 weeks (**A**), 32 weeks (**B**) and 43 weeks (**C**), with a scale bar of 50 μm; **D**: Lung tissue β-gal staining statistics; **E-G**: Increased expression of *GLB1* (**E**), *P16* (**F**), and *P21* (**G**) genes in lung tissues of 32-week-old and 43- week-old compared to 12-week-old mice. Data are presented as the mean ± SEM ($n = 6$), with $^{\#}P > 0.05$, $^{*}P < 0.05$, $^{**}P < 0.01$, $^{***}P < 0.001$.

pulmonary fibrosis, facilitating the study of its underlying mechanisms.

This study confirmed the PF characteristic phenotype in naturally aging NOD/SCID mice at 12 weeks, 32 weeks, and 43 weeks by testing HE staining, Masson staining, α-SMA immunohistochemistry, and hydroxyproline content in lung tissue. Masson staining of lung tissue from mice aged 32 and 43 weeks revealed only minimal collagen deposition in the lung parenchyma, with no significant differences between these age groups; moreover, the levels of hydroxyproline in lung tissue from mice aged 32 and 43 weeks did not show statistical significance either; however, both Masson staining and hydroxyproline levels were higher than those in 12-week-old mice. These results suggest that while NOD/SCID mice at 12, 32, and 43 weeks all exhibit the PF phenotype, there are no significant differences in the Masson staining and hydroxyproline levels between 32 and 43 weeks. This may be due to the small sample size included in the study or related to the aging process in NOD/SCID mice Above findings align with the characteristics of bleomycin-induced in young mouse models (6 to 10 weeks old) reported in previous studies [13, 37]. Despite these similarities, the inflammation and fibrosis of lung tissue in naturally aged NOD/SCID mice worsened with increasing age (Figs. 1 and 2), reflecting two clinical characteristics of human IPF: gradual aggravation and irreversibility. In contrast, young C57 mouse models of PF induced by bleomycin (6 to 8 weeks old) were failed to replicate the gradual and irreversible deterioration observed in human IPF with aging [38].

Transforming growth factor-β (TGF-β) has been identified as a key factor in pulmonary fibrosis, through its regulation of fibroblast differentiation and proliferation [39]. Additionally, pro-inflammatory factors such as IL-6 and TNF-α play crucial roles in the regulation of inflammation and pulmonary fibrosis [3], while IL-1β also implicated in the pathogenesis of the disease [28]. IL-8 is considered a potential mediator of fibrotic mesenchymal progenitor cell fibrosis and a driver of fibrosis progression [40]. In context of bleomycin-induced PF, the expression levels of *TGF-β1*, *TNF-α*, *IL-6*, *IL-1β*, and *IL-8* genes are known to increase [28]. Our study found that the expression levels of these inflammation-related genes in the lung tissue of NOD/SCID mice aged 32 weeks and 43 weeks were higher than those observed at 12 weeks of

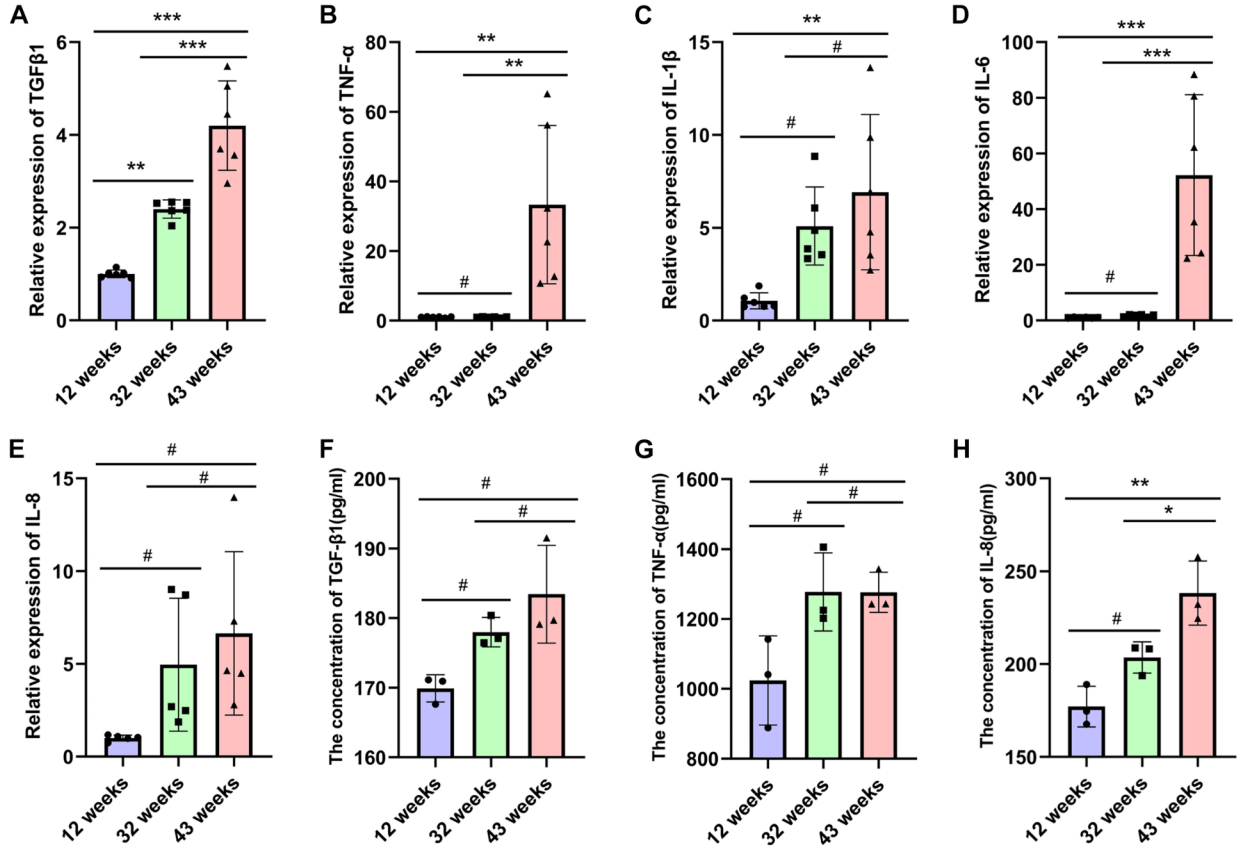

Fig. 4 illustrates the increased expression of pro-inflammatory related genes in the lung tissue of experimental mice with advancing age. The expression levels of inflammatory genes *TGF-β1* (**A**), *TNF-α* (**B**), *IL-1β* (**C**), *IL-6* (D) and *IL-8* (**E**) in lung tissues of mice from each group were quantified using quantitative PCR. Data are presented as the mean ± SEM ($n = 6$). $^{**}P < 0.01$, $^{***}P < 0.001$. The expression levels of inflammatory proteins TGF-β1 (**F**), TNF-α (**G**), IL-8 (**H**) in lung tissues of mice from each group were detected by ELISA. Data are presented as the mean ± SEM ($n = 3$). $^{\#}P > 0.05$, $^{*}P < 0.05$, $^{**}P < 0.01$.

age (Fig. 4). Furthermore, the expression levels of these genes increased gradually with the age of the mice. These findings are consistent with previous reports indicating a significant elevation in the concentration of TGF-β1 in peripheral blood mononuclear cells from elderly IPF patients [41]. However, due to challenges with collecting peripheral blood mononuclear cells from mice, this study did not measure the concentration of TGF-β1 in these cells.

Oxidative stress is recognized as a key pathogenic factor in pulmonary fibrosis [29]. The nuclear factor erythroid 2-related factor 2 (Nrf2) plays a crucial role in maintaining cellular REDOX homeostasis [30]. Upon stimulation, Nrf2 undergoes phosphorylation, leading to its dissociation from the Kelch-like ECH-associated protein 1 (Keap1) and translocation into the nucleus, where it activates the transcription of antioxidant enzymes such as SOD1/2 [42]. Studies have demonstrated that the activity of SOD1/2 in Nrf2-knockout mice is significantly reduced compared to wild-type mice 24 h after heart allograft reperfusion [43]. SOD1 and SOD2 are essential antioxidant enzymes that convert ROS into oxygen or hydrogen peroxide, thereby helping to prevent lung damage and fibrosis [44]. Sirtuins, a family of nicotinamide adenine dinucleotide (NAD)+dependent protein deacetylases, play critical roles in lung aging and disease. SIRT1 inhibits cellular senescence and fibrosis, while SIRT3 is recognized for its anti-fibrotic properties [45]. Both SIRT1 and SIRT3 protect cells from ROS damage [32]. Previous studies have reported decreased expression levels of SOD1, SOD2, NRF2, SIRT1, and SIRT3 in the lung tissue of C57 mouse models aged 6–10 weeks with bleomycin-induced PF [46–48]. Our study found that the mRNA levels of *SOD1*, *SOD2*, *NRF2*, *SIRT1*, and *SIRT3* in the lung tissue of NOD/SCID mice decreased with increasing age (Fig. 5). Furthermore, the expression levels of these anti-oxidative stress-related genes in mice aged 43 weeks were lower than those in mice aged 32 weeks. These findings align with previous reports indicating a significant decrease in the concentration of SIRT1 in peripheral blood mononuclear cells from elderly patients with IPF, as well as reduced expression of SIRT3 in the lungs of clinical subjects with IPF [41, 48]. However, due

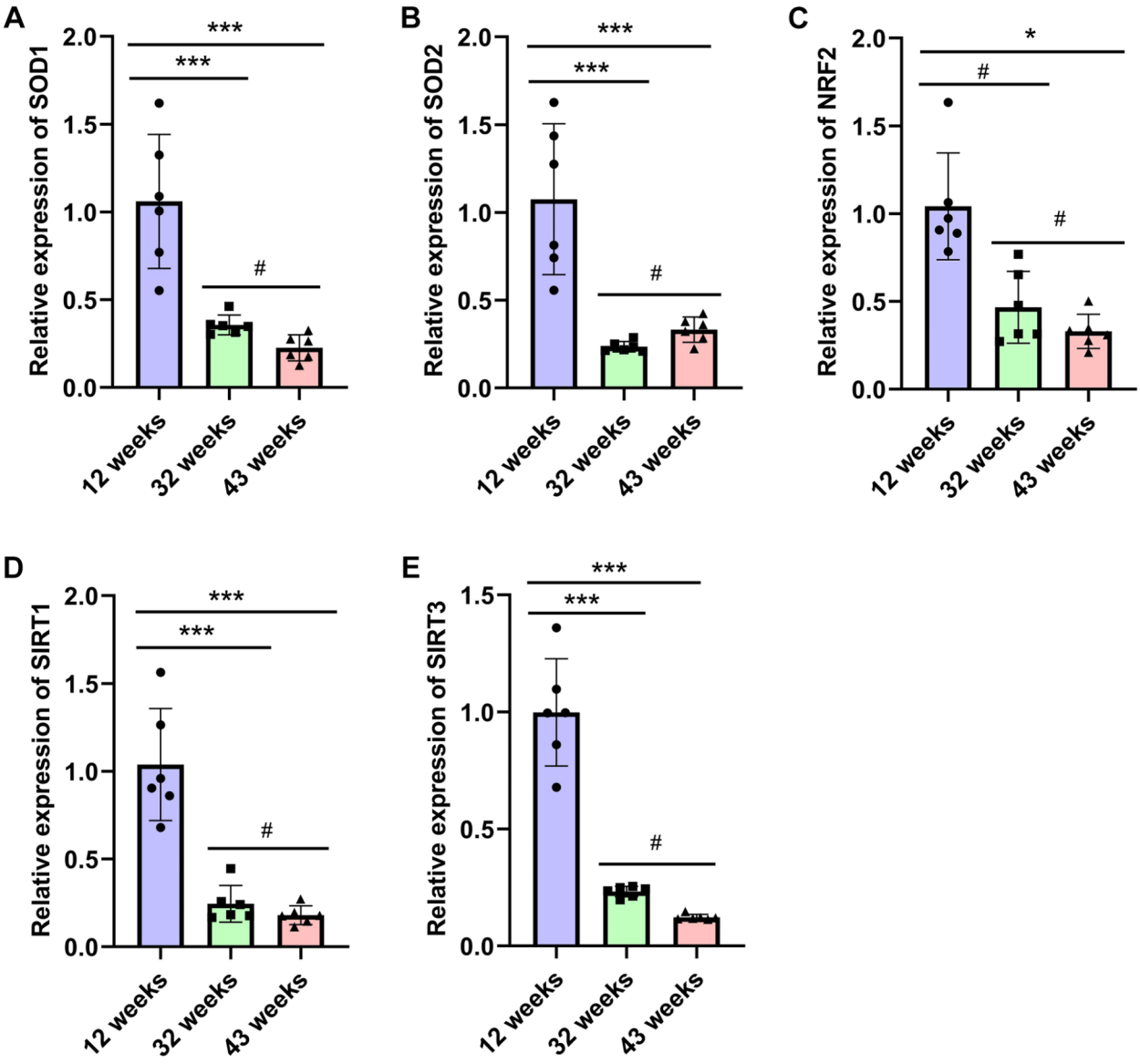

Fig. 5 illustrates the gradual decrease in the expression of antioxidant stress-related genes in the lung tissue of experimental mice with increasing age. The expression levels of anti-oxidative stress-related genes *SOD1* (**A**), *SOD2* (**B**), *NRF2* (**C**), *SIRT1* (**D**) and *SIRT3* (**E**) in lung tissue of mice from each group were quantified using quantitative PCR. Data are presented as the mean ± SEM ($n = 6$), with $^{\#}P > 0.05$, $^{*}P < 0.01$, $^{**}P < 0.01$, $^{***}P < 0.001$.

to challenges in mouse peripheral blood mononuclear cells were not measured in this study.

Although the NOD/SCID mice at 32 and 43 weeks of age have a clear PF phenotype, the long modeling time required for this PF animal model may lead to increased costs; additionally, the immune deficiency characteristics of NOD/SCID mice and the mechanisms of onset or development of PF diseases still require further study.

Conclusions

Our results indicate that naturally aged NOD/SCID mice at 32 and 43 weeks of age can serve as models for studying idiopathic pulmonary fibrosis (IPF) in the elderly population. The pathogenesis observed in this model appears to be closely associated with aging, inflammation, and oxidative stress. Given that naturally aged NOD/SCID mice exhibit a disease that mirrors human IPF, along with histopathological and molecular characteristics consistent with the gradual progression and irreversibility seen in human cases, they represent a stable and reliable animal model for investigating human IPF. Moreover, the immunodeficient nature of NOD/SCID mice suggests that this model could be particularly valuable for preclinical studies involving autologous cell interventions. However, it is important to note that the average lifespan of NOD/SCID mice is approximately

8.5 months (or roughly 35 weeks), and natural mortality tends to increase after 38 weeks in our experiments. This study found that both 32-week-old and 43-week-old NOD/SCID mice exhibit the PF phenotype, but there are no significant differences in Masson staining and hydroxyproline levels between these ages. Therefore, especially in pharmacological research and autologous cell drug studies, we recommend using 32-week-old NOD/SCID mice as the PF animal model.

Abbreviations

IL-1β	Interleukin-1β
IL-6	Interleukin-6
IL-8	Interleukin-8
IPF	Idiopathic Pulmonary Fibrosis
MMP9	Matrix Metalloproteinase 9
NRF2	Nuclear factor erythroid 2-related factor 2
SIRT1	Sirtuins 1
SIRT3	Sirtuins 3
SOD1	Superoxide Dismutase 1
SOD2	Superoxide Dismutase 2
TGF-β	Transforming Growth Factor-β
TNF-α	Tumor Necrosis Factor α

Supplementary Information

The online version contains supplementary material available at https://doi.org/10.1186/s12890-024-03268-3.

Supplementary Material 1

Acknowledgements
Not applicable.

Author contributions
Y.L., Z.M. and M.H.contributed to the study design. Z.M., L.Q. and Y. L. were responsible for organizing the study. S. L. conducted the animal feeding and sampling. Y. Z. performed quantitative PCR detection. J.Y. and S.Y. carried out the pathology experiments. Z.M., L.Q., J.S. and Z.W. sorted and analyzed the data. Z.M. and L.Q. completed the manuscript. Y.L. and M.H. revised the manuscript. All authors reviewed and approved the final version of the manuscript together.

Funding
This work was supported by the Talent Research Project of Kunming University (YJL23012) and Yunnan Key Laboratory of Basic Research for Bone and Joint Diseases (202205AG070075).

Data availability
The datasets from this study are available. Please contact the corresponding author to request access.

Declarations

Ethics approval and consent to participate
This study was conducted following the ARRIVE guidelines. The Experimental Animal Welfare and Ethics Committee of Kunming University granted approval for all animal experiments (approval number: 2021kmu011). All operations were performed under anesthesia while efforts were made to minimize suffering to the animals.

Consent to publish
Not applicable.

Competing interests
The authors declare no competing interests.

Author details
[1]Yunnan Key Laboratory for Basic Research on Bone and Joint Diseases, Kunming University, Kunming, Yunnan 650214, China
[2]Yunnan Jici Institute for Regenerative Medicine Co., Ltd, Kunming, Yunnan 650101, China
[3]Shenzhen Zhendejici Pharmaceutical Research and Development Co., Ltd, Shenzhen 518048, Guangdong, China

Received: 22 April 2024 / Accepted: 4 September 2024
Published online: 16 September 2024

References

1. Richeldi L, Collard HR, Jones MG. Idiopathic pulmonary fibrosis. Lancet. 2017;389(10082):1941–52.
2. Ayilya BL, Balde A, Ramya M, Benjakul S, Kim SK, Nazeer RA. Insights on the mechanism of bleomycin to induce lung injury and associated in vivo models: a review. Int Immunopharmacol. 2023;121:110493.
3. Zhang J, Li Q, Shao Q, Song J, Zhou B, Shu P. Effects of panax notoginseng saponin on the pathological ultrastructure and serum IL-6 and IL-8 in pulmonary fibrosis in rabbits. J Cell Biochem. 2018;119(10):8410–8.
4. Shi X, Li XJ, Sun XY, Cui W, Liu HG, Xu SW. Pig lung fibrosis is active in the subacute CdCl2 exposure model and exerts cumulative toxicity through the M1/M2 imbalance. Ecotoxicol Environ Saf. 2021;225:112757.
5. Organ L, Bacci B, Koumoundouros E, Barcham G, Milne M, Kimpton W, Samuel C, Snibson K. Structural and functional correlations in a large animal model of bleomycin-induced pulmonary fibrosis. BMC Pulm Med. 2015;15:81.
6. Che P, Wang M, Larson-Casey JL, Hu RH, Cheng Y, El Hamdaoui M, Zhao XK, Grytz R, Brent Carter A, Ding Q. A novel tree shrew model of pulmonary fibrosis. Lab Invest. 2021;101(1):116–24.
7. Vellichirammal NN, Sethi S, Pandey S, Singh J, Wise SY, Carpenter AD, Fatanmi OO, Guda C, Singh VK. Lung transcriptome of nonhuman primates exposed to total- and partial-body irradiation. Mol Ther Nucleic Acids. 2022;29:584–98.
8. Meyerholz DK. Lessons learned from the cystic fibrosis pig. Theriogenology. 2016;86(1):427–32.
9. Plog S, Grötzsch T, Klymiuk N, Kobalz U, Gruber AD, Mundhenk L. The porcine chloride channel calcium-activated family member pCLCA4a mirrors lung expression of the human hCLCA4. J Histochem Cytochem. 2012;60(1):45–56.
10. Moore BB, Hogaboam CM. Murine models of pulmonary fibrosis. Am J Physiol Lung Cell Mol Physiol. 2008;294(2):L152–60.
11. Sueblinvong V, Neveu WA, Neujahr DC, Mills ST, Rojas M, Roman J, Guidot DM. Aging promotes pro-fibrotic matrix production and increases fibrocyte recruitment during acute lung injury. Adv Biosci Biotechnol. 2014;5(1):19–30.
12. Torres-González E, Bueno M, Tanaka A, Krug LT, Cheng DS, Polosukhin VV, Sorescu D, Lawson WE, Blackwell TS, Rojas M, Mora AL. Role of endoplasmic reticulum stress in age-related susceptibility to lung fibrosis. Am J Respir Cell Mol Biol. 2012;46(6):748–56.
13. Zhao X, Wu J, Yuan R, Li Y, Yang Q, Wu B, Zhai X, Wang J, Magalon J, Sabatier F, Daumas A, Zhu WM, Zhu N. Adipose-derived mesenchymal stem cell therapy for reverse bleomycin-induced experimental pulmonary fibrosis. Sci Rep. 2023;13(1):13183.
14. Periera-Simon S, Xia X, Catanuto P, Coronado R, Kurtzberg J, Bellio M, Lee YS, Khan A, Smith R, Elliot SJ, Glassberg MK. Anti-fibrotic effects of different sources of MSC in bleomycin-induced lung fibrosis in C57BL6 male mice. Respirology. 2021;26(2):161–70.
15. Cheng W, Zeng Y, Wang D. Stem cell-based therapy for pulmonary fibrosis. Stem Cell Res Ther. 2022;13(1):492.
16. Zhang Y, Tang WY, Su XW, Dong BX, Wang Q, Wang ZY, Yang YX, Qu SQ, Luan Z. Immunological effects of the intraparenchymal administration of allogeneic and autologous adipose-derived mesenchymal stem cells after the acute phase of middle cerebral artery occlusion in rats. J Transl Med. 2018;16(1):339.
17. Ankrum JA, Ong JF, Karp JM. Mesenchymal stem cells: immune evasive, not immune privileged. Nat Biotechnol. 2014;32(3):252–60.
18. Chen J, Liao S, Xiao Z, Pan Q, Wang X, Shen K, Wang S, Yang L, Guo F, Liu HF, Pan Q. The development and improvement of immunodeficient mice and humanized immune system mouse models. Front Immunol. 2022;13:1007579.
19. Marchante M, Ramirez-Martin N, Buigues A, Martinez J, Pellicer N, Pellicer A, Herraiz S. Deciphering reproductive aging in women using a NOD/

SCID mouse model for distinct physiological ovarian phenotypes. Aging. 2023;15(20):10856–74.
20. Okada S, Vaeteewoottacharn K, Kariya R. Application of highly immunocompromised mice for the establishment of patient-derived xenograft (PDX) models. Cells. 2019;8(8):889.
21. Li D, Li P, He Z, Meng Z, Luo X, Fang J. Establishment of NOD/SCID mouse model of central nervous system leukemia. Oncol Rep. 2014;32(2):684–90.
22. Huang SY, Tien HF, Su FH, Hsu SM. Nonirradiated NOD/SCID-human chimeric animal model for primary human multiple myeloma: a potential in vivo culture system. Am J Pathol. 2004;164(2):747–56.
23. Zhang B, Li Y, Zhong X, Huang W, Nie L, Zhang W. Establishment of retinoblastoma model in NOD-SCID mice and study of metastasis. Yan Ke Xue Bao. 2005;21(3):185–91.
24. Fisher S, Burgess WL, Hines KD, Mason GL, Owiny JR. Interstrain differences in CO2-induced pulmonary hemorrhage in mice. J Am Assoc Lab Anim Sci. 2016;55(6):811–5.
25. Ashcroft T, Simpson JM, Timbrell V. Simple method of estimating severity of pulmonary fibrosis on a numerical scale. J Clin Pathol. 1988;41(4):467–70.
26. Espindola MS, Habiel DM, Coelho AL, Stripp B, Parks WC, Oldham J, Martinez FJ, Noth I, Lopez D, Mikels-Vigdal A, Smith V, Hogaboam CM. Differential responses to targeting matrix metalloproteinase 9 in idiopathic pulmonary fibrosis. Am J Respir Crit Care Med. 2021;203(4):458–70.
27. Xiong Y, Cui X, Zhou Y, Chai G, Jiang X, Ge G, Wang Y, Sun H, Che H, Nie Y, Zhao P. Dehydrocostus lactone inhibits BLM-induced pulmonary fibrosis and inflammation in mice via the JNK and p38 MAPK-mediated NF-κB signaling pathways. Int Immunopharmacol. 2021;98:107780.
28. Otoupalova E, Smith S, Cheng G, Thannickal VJ. Oxidative stress in pulmonary fibrosis. Compr Physiol. 2020;10(2):509–47.
29. Kinnula VL, Fattman CL, Tan RJ, Oury TD. Oxidative stress in pulmonary fibrosis: a possible role for redox modulatory therapy. Am J Respir Crit Care Med. 2005;172(4):417–22.
30. Hecker L, Logsdon NJ, Kurundkar D, Kurundkar A, Bernard K, Hock T, Meldrum E, Sanders YY, Thannickal VJ. Reversal of persistent fibrosis in aging by targeting Nox4-Nrf2 redox imbalance. Sci Transl Med. 2014;6(231):231ra47.
31. Watanabe K, Shibuya S, Ozawa Y, Nojiri H, Izuo N, Yokote K, Shimizu T. Superoxide dismutase 1 loss disturbs intracellular redox signaling, resulting in global age-related pathological changes. Biomed Res Int. 2014;2014:140165.
32. Singh CK, Chhabra G, Ndiaye MA, Garcia-Peterson LM, Mack NJ, Ahmad N. The role of sirtuins in antioxidant and redox signaling. Antioxid Redox Signal. 2018;28(8):643–61.
33. Rojas M, Xu J, Woods CR, Mora AL, Spears W, Roman J, Brigham KL. Bone marrow-derived mesenchymal stem cells in repair of the injured lung. Am J Respir Cell Mol Biol. 2005;33(2):145–52.
34. Dinh PC, Paudel D, Brochu H, Popowski KD, Gracieux MC, Cores J, Huang K, Hensley MT, Harrell E, Vandergrif AC, et al. Inhalation of lung spheroid cell secretome and exosomes promotes lung repair in pulmonary fibrosis. Nat Commun. 2020;11(1):1064.
35. Lei X, He N, Zhu L, Zhou M, Zhang K, Wang C, Huang H, Chen S, Li Y, LiuQ, et al. Mesenchymal stem cell-derived extracellular vesicles attenuate radiation-induced lung injury via miRNA-214-3p. Antioxid Redox Signal. 2021;35(11):849–62.
36. Willis GR, Fernandez-Gonzalez A, Reis M, Yeung V, Liu X, Ericsson M, Andrews NA, Mitsialis SA, Kourembanas S. Mesenchymal stromalcell-derived small extracellular vesicles restore lung architecture and improve exercise capacity in a model of neonatal hyperoxia-induced lung injury. J Extracell Vesicles. 2020;9(1):1790874.
37. Zou L, Hong D, Li K, Jiang B. Salt-inducible kinase 2 (SIK2) inhibitor ARN-3236 attenuates bleomycin-induced pulmonary fibrosis in mice. BMC Pulm Med. 2022;22(1):140.
38. Li S, Shi J, Tang H. Animal models of drug-induced pulmonary fibrosis: an overview of molecular mechanisms and characteristics. Cell Biol Toxicol. 2022;38(5):699–723.
39. Zhang Y, Jiao H, Wu Y, Sun X. P120-catenin regulates pulmonary fibrosis and TGF-β induced lung fibroblast differentiation. Life Sci. 2019;230:35–44.
40. Yang L, Herrera J, Gilbertsen A, Xia H, Smith K, Benyumov A, Bitterman PB, Henke CA. IL-8 mediates idiopathic pulmonary fibrosis mesenchymal progenitor cell fibrogenicity. Am J Physiol Lung Cell Mol Physiol. 2018;314(1):L127–36.
41. Deskata K, Malli F, Jagirdar R, Vavougios GD, Zarogiannis S, Gourgoulianis KI, Daniil Z. Evaluation of Sirtuin 1 levels in peripheral blood mononuclear cells of patients with idiopathic pulmonary fibrosis. Cureus. 2022;14(10):e30862.
42. Aparici M, Bravo M, Calama E, García-González V, Domènech T, Córdoba M, Roger I, Cortijo J, Góngora-Benítez M, Paradís-Bas M, Collins B, Davis AM, Albericio F, Puig C. Pharmacological characterization of a novel peptide inhibitor of the Keap1-Nrf2 protein-protein interaction. Biochem Pharmacol. 2022;204:115226.
43. Fukunaga N, Kawajiri H, Badiwala MV, Butany J, Li RK, Billia F, Rao V. Protective role of Nrf2 against ischemia reperfusion injury and cardiac allograft vasculopathy. Am J Transpl. 2020;20(5):1262–71.
44. Kim NH, Kim HY, Lee JH, Chang I, Heo SH, Kim J, Kim JH, Kang JH, Lee SW. Superoxide dismutase secreting Bacillus amyloliquefaciens spores attenuate pulmonary fibrosis. Biomed Pharmacother. 2023;168:115647.
45. Shaikh SB, Prabhu A, Bhandary YP. Targeting anti-aging protein sirtuin (sirt) in the diagnosis of idiopathic pulmonary fibrosis. J Cell Biochem. 2019;120(5):6878–85.
46. Lan YW, Chen YC, Yen CC, Chen HL, Tung MC, Fan HC, Chen CM. Kefir peptides mitigate bleomycin-induced pulmonary fibrosis in mice through modulating oxidative stress, inflammation and gut microbiota. Biomed Pharmacother. 2024;174:116431.
47. Chien LH, Deng JS, Jiang WP, Chou YN, Lin JG, Huang GJ. Evaluation of lung protection of Sanghuangporus sanghuang through TLR4/NF-κB/MAPK, keap1/Nrf2/HO-1, CaMKK/AMPK/Sirt1, and TGF-β/SMAD3 signaling pathways mediating apoptosis and autophagy. Biomed Pharmacother. 2023;165:115080.
48. Rehan M, Kurundkar D, Kurundkar AR, Logsdon NJ, Smith SR, Chanda D, Bernard K, Sanders YY, Deshane JS, Dsouza KG, Rangarajan S, Zmijewski JW, Thannickal VJ. Restoration of SIRT3 gene expression by airway delivery resolves age-associated persistent lung fibrosis in mice. Nat Aging. 2021;1(2):205–17.

Publisher's note